Collective excitations in cigar-shaped spin-orbit-coupled spin-1 Bose-Einstein condensates

Rajat,[1,*] Arko Roy,[2,3,†] and Sandeep Gautam [1,‡]

[1]*Department of Physics, Indian Institute of Technology Ropar, Rupnagar 140001, Punjab, India*
[2]*INO-CNR BEC Center and Università di Trento, Via Sommarive 14, 38123 Trento, Italy*
[3]*School of Basic Sciences, Indian Institute of Technology Mandi, Mandi 175075, Himachal Pradesh, India*

We study theoretically the collective excitations of a spin-orbit-coupled spin-1 Bose-Einstein condensate with antiferromagnetic spin-exchange interactions in a cigar-shaped trapping potential at zero and finite temperatures using the Hartree-Fock-Bogoliubov theory with Popov approximation. The collective modes at zero temperature are corroborated by real-time evolution of the ground state subjected to a perturbation suitable to excite a density or a spin mode. We also calculate a few low-lying modes analytically and find very good agreement with the numerical results. We confirm the presence of excitations belonging to two broad categories, namely, density and spin excitations, based on the calculation of dispersion. The degeneracy between a pair of spin modes is broken by the spin-orbit coupling. At finite temperature, spin and density excitations show qualitatively different behavior as a function of temperature.

I. INTRODUCTION

The first multicomponent Bose-Einstein condensate (BEC), known as a spinor condensate, was experimentally realized with a simultaneous optical trapping of three hyperfine spin states from the $F = 1$ spin manifold in a gas of ^{23}Na atoms [1] and was followed by the demonstration of the condensation with gas of ^{87}Rb atoms in $F = 1$ [2] and $F = 2$ [3–5] manifolds. The vast literature on the spinor condensates covering both the experimental and the theoretical progress has been reviewed in Refs. [6,7]. One of the most important advances in the field of cold-atom physics in the past decade has been the experimental demonstration of synthetic spin-orbit (SO) coupling in a pseudospin-half quantum gas [8] via light-atom interactions, which has opened up new perspectives in exploring many-body phenomena using ultracold atoms, such as topological insulators [9], quantum anomalous Hall conductivity [10], and topological superconductors [11]. In the case of spin-1 BECs, SO coupling has also been experimentally realized in a gas of ^{87}Rb [12,13] atoms by coupling three hyperfine states with Raman lasers, thus paving the way to explore the rich physics of SO-coupled spin-1 BECs. Theoretical predictions and experimental observations of SO-coupled spin-1 BECs render various novel ground-state phases including plane-wave, stripe (standing-wave), and zero-momentum phases [14,15]. Distinguishing the different phases close to the phase-transition boundaries through equilibrium density profiles is a challenge [16]. Nonequilibrium transport of spinor BECs entails various topological excitations such as solitons [17] and vortices [17,18]. To characterize the

static and dynamical properties of such systems, it is then imperative to study the collective excitations manifesting through fluctuations.

Collective modes, which are the low-energy excitations of a quantum gas, can reveal fundamental information about the ultracold quantum state such as the stability of different different ground-state phases, fluctuations, and superfluidity [19,20]. To this end, it is experimentally possible to excite the low-lying dipole and breathing modes by modulating the harmonic trap and carry out spectroscopic studies with utmost precision [21]. At zero temperature, the collective excitations of the trapless pseudospinor and spin-1 BECs with Raman-induced SO coupling have been studied theoretically [22–24] and have been found to exhibit roton-maxon structure in zero-momentum and plane-wave phases. Dynamical and energetic instabilities in the Raman-induced SO-coupled pseudospinor BEC in a uniform plane-wave phase have also been studied [25]. Experimental measurement of collective excitations through Bragg spectroscopy in Raman-induced SO-coupled pseudospinor BECs, revealing the roton-maxon structure, have been carried out [26,27]. The excitation spectrum of a one-dimensional quantum droplet for a binary mixture has been examined in Ref. [28]. In contrast, theoretical studies of spinor condensates at finite temperatures are few and demand a thorough investigation. Experiments usually are performed in harmonic traps and at finite temperatures. It is therefore essential to include the effects of the trapping potential and fluctuations to theoretically address such systems. It has been shown that an antiferromagnetic spin-1 Bose gas with fixed norm and magnetization undergoes double condensation using Hartree-Fock-Popov [29] and Hartree-Fock theories [30]. Phuc *et al.* [31] have studied the finite-temperature phase diagram of a trapless ferromagnetic spin-1 Bose gas in the presence of quadratic Zeeman terms using Hartree-Fock-Bogoliubov theory with Popov approximation. Within the framework of Hartree-Fock theory, the

*rajat.19phz0009@iitrpr.ac.in
†arko@iitmandi.ac.in
‡sandeep@iitrpr.ac.in

finite-temperature phase diagram of a trapless spin-1 BEC with both linear and quadratic Zeeman terms has also been calculated [32]. Experimentally, the phase diagram of an anti-ferromagnetic spin-1 Bose gas has been studied in Ref. [33]. The spin-mixing dynamics of a spin-1 condensate in a highly elongated trap has been studied at zero and finite temperature [34,35]. The effect of thermal fluctuations on the quantum phase transition from an antiferromagnetic to phase-separated ground state in a spin-1 BEC has been studied in [36]. The finite-temperature phase diagram of a uniform pseudospinor-half BEC with a Raman-induced SO coupling shows that quantum and thermal fluctuations enlarge the phase space of a plane-wave phase [37]. A finite-temperature phase transition from a stripe to a plane-wave phase in a Raman-induced SO-coupled pseudospinor-half ^{87}Rb Bose gas has been experimentally observed [38]. A perturbation approach, valid for small Raman coupling strengths, has been used to study the transition between the plane-wave and stripe phases for a Raman-induced SO-coupled pseudospinor-half BEC at finite temperatures [39]. The stability of the plane-wave phase in the Rashba SO-coupled pseudospinor condensate with equal intra- and interspecies interactions against quantum and thermal fluctuations has been studied [40]. The Berezinskii-Kosterlitz-Thouless (BKT) superfluid phase transition in an anisotropically SO-coupled two-dimensional pseudospinor BEC has been studied using classical-field Monte Carlo calculations [41] and the stochastic projected Gross-Pitaevskii equation [42]; the latter study showed the emergence of a true long-range order in the relative phase sector and the quasi-long-range BKT order in the total phase sector [42].

In this work we study theoretically the collective excitations of an SO-coupled spin-1 BEC, with antiferromagnetic spin-exchange interactions, in a quasi-one-dimensional harmonic trapping potential at zero and finite temperature using the Hartree-Fock-Bogoliubov (HFB) theory with Popov approximation. Excitation spectra of SO-coupled spin-1 BECs in harmonic trapping potentials have not been studied at zero or finite temperature. We calculate the collective excitation spectrum by numerically solving the generalized Gross-Pitaevskii (GP) and Bogoliubov–de Gennes (BdG) equations self-consistently at zero and finite temperatures. In addition to this at $T = 0$ K, we also calculate the collective oscillations by simulating the real-time propagation of the ground state using $T = 0$ GP equations subjected to different kinds of spin and density perturbations. We also calculate the dispersion relation [43] to ascertain the nature of the excitations. To augment our numerical results, we use the variational method to calculate the frequencies of a few low-lying modes analytically.

The paper is organized as follows. In Sec. II we describe the HFB theory with Popov approximation for an SO-coupled spin-1 BEC in a quasi-one-dimensional trapping potential. In Sec. III A we discuss the spectrum of the noninteracting SO-coupled spin-1 BEC. We calculate the collective excitation of an SO-coupled spin-1 BEC of ^{23}Na at zero temperature with and without SO coupling by solving the generalized GP and BdG equations in a self-consistent manner in Secs. III B and III C. In Sec. III D we simulate the real-time dynamics of a suitably perturbed ground state to monitor the dipole and breathing modes corresponding to density and spin channels,

followed by a calculation of a few low-lying modes using the variational method in Sec. III E. In Sec. IV the excitation spectra at finite temperatures are discussed.

II. MODEL

We consider a spin-1 SO-coupled spinor BEC in a highly anisotropic harmonic trapping potential $V(x, y, z) = m(\omega_x^2 x^2 + \omega_y^2 y^2 + \omega_z^2 z^2)/2$, where m is the atomic mass and $\omega_y = \omega_z = \omega_\perp \gg \omega_x$. The transverse degrees of freedom are then considered to be frozen and the system is confined in the harmonic-oscillator ground state along this direction with $R_x \gg \xi \gg l_\perp$, where R_x is the half-length of the condensate along the x axis, ξ is the density-coherence length, and $l_\perp = \sqrt{\hbar/m\omega_\perp}$. In this case, we can integrate out the y and z coordinates from the condensate wave function and describe the system as a quasi-one-dimensional system along the x axis. This allows us to consider excitations only along the axial direction x. The grand-canonical Hamiltonian in the second-quantized form for a spin-1 BEC is $\mathcal{H} = \mathcal{H}_0 + \mathcal{H}_{int}$, where single-particle part of the Hamiltonian $\mathcal{H}_0$ and interaction part of the Hamiltonian $\mathcal{H}_{int}$ are [44,45]

$$\mathcal{H}_0 = \int dx \, \hat{\psi}_i^\dagger [\mathcal{L}_{ij} - i\hbar\gamma f_x \partial_x] \hat{\psi}_j, \tag{1a}$$

$$\mathcal{H}_{int} = \int dx \left[\frac{c_0}{2} \hat{\psi}_i^\dagger \hat{\psi}_j^\dagger \hat{\psi}_j \hat{\psi}_i + \frac{c_2}{2} \hat{\psi}_i^\dagger (f_\alpha)_{ij} \hat{\psi}_j \hat{\psi}_k^\dagger (f_\alpha)_{kl} \hat{\psi}_l \right], \tag{1b}$$

where $\partial_x = \partial/\partial x$ and $\mathcal{L}_{ij} = [(-\hbar^2/2m)\partial_x^2 - \mu + V(x)]\delta_{ij}$. In Eqs. (1a) and (1b), i, j, k, l, which can have values $+1$, 0, -1, are the hyperfine spin states of the $F = 1$ manifold; repeated indices are summed over; f_α with $\alpha = x, y, z$ denote the spin-1 matrices in the irreducible representation; $\hat{\psi}_i(x, t)[\hat{\psi}_i^\dagger(x, t)]$ is the quantum field for annihilating (creating) an atom in state i at position x; μ is the chemical potential; γ is the strength of spin-orbit coupling; and c_0 and c_2 are spin-independent and spin-dependent interactions, respectively, which, expressed in terms of the s-wave scattering lengths a_0 and a_2 of binary collisions with total spin $F_{total} = 0$ and 2, respectively, are $c_0 = 2\hbar^2(a_0 + 2a_2)/3ml_\perp^2$ and $c_2 = 2\hbar^2(a_2 - a_0)/3ml_\perp^2$. Depending on the values of c_2, a spin-1 BEC in the absence of SO coupling and Zeeman terms admits two phases, namely, ferromagnetic for $c_2 < 0$ and antiferromagnetic for $c_2 > 0$. In the rest of the paper we will work with dimensionless variables (except when stated otherwise) defined as $\tilde{x} = x/l_0$, $\tilde{E} = E/\hbar\omega_x$, $\tilde{t} = \omega_x t$, $\tilde{\gamma} = \gamma/\sqrt{m\hbar\omega_x}$, $\tilde{c}_0 = 2(a_0 + 2a_2)l_0/3l_\perp^2$, and $\tilde{c}_2 = 2(a_2 - a_0)l_0/3l_\perp^2$, where $l_0 = \sqrt{\hbar/m\omega_x}$; we further denote the dimensionless variables without a tilde in the rest of the paper.

Fluctuations

To address the effects of quantum and thermal fluctuations in the BECs of dilute atomic gases, we generalize the HFB theory within the Popov approximation [46–48] and adapt it to an SO-coupled spin-1 Bose gas. We start with the second-quantized form of the Hamiltonian $\mathcal{H}$ for a dilute, weakly interacting Bose gas and derive the generalized GP and the BdG equations. We separate the Bose field operator $\hat{\psi}_i(x, t)$

into a condensate wave function $\phi_i(x)$ and a fluctuation operator $\delta\hat{\psi}_i(x,t)$ as $\hat{\psi}_i(x,t) = \phi_i(x) + \delta\hat{\psi}_i(x,t)$. Employing the Bogoliubov transformation, fluctuation operators $\delta\hat{\psi}_i$ can be expressed as a linear combination of quasiparticle creation ($\hat{\alpha}_\lambda^\dagger$) and annihilation operators ($\hat{\alpha}_\lambda$) given by

$$\delta\hat{\psi}_i(x,t) = \sum_\lambda [u_i^\lambda(x)\hat{\alpha}_\lambda(x)e^{-i\omega_\lambda t} - v_i^{*\lambda}(x)\hat{\alpha}_\lambda^\dagger(x)e^{i\omega_\lambda t}], \quad (2)$$

where $i \in (+1, 0, -1)$ represents the component index and λ represents the eigenvalue index for the corresponding energy ω_λ, with u_i^λ and v_i^λ the quasiparticle amplitudes of the ith component. The quasiparticle creation and annihilation operators satisfy the usual Bose commutation relations. We consider the Heisenberg equation for the Bose field operator $\hat{\psi}_i(x,t)$, i.e.,

$$i\hbar\frac{\partial}{\partial t}\hat{\psi}_i(x,t) = [\hat{\psi}_i(x,t), \mathcal{H}], \quad (3)$$

and then Wick decompose the cubic terms in fluctuation operators as $\delta\hat{\psi}_i^\dagger \delta\hat{\psi}_j \delta\hat{\psi}_k \simeq \langle\delta\hat{\psi}_i^\dagger \delta\hat{\psi}_j\rangle\delta\hat{\psi}_k + \langle\delta\hat{\psi}_i^\dagger \delta\hat{\psi}_k\rangle\delta\hat{\psi}_j + \langle\delta\hat{\psi}_j \delta\hat{\psi}_k\rangle\delta\hat{\psi}_i^\dagger$. We consider the ensemble average of Eq. (3) and define $n_i^c = |\phi_i|^2$, $\tilde{n}_{i,j} \equiv \langle\delta\hat{\psi}_i^\dagger \delta\hat{\psi}_j\rangle$, $\tilde{m}_{i,j} \equiv \langle\delta\hat{\psi}_i \delta\hat{\psi}_j\rangle$, and $n_i = n_i^c + \tilde{n}_{i,i}$ as the local condensate, noncondensate, anomalous, and total densities, respectively, for the ith component and $n_t = \sum_i(n_i^c + \tilde{n}_{i,i})$ as the total density of the system. To simplify the notation, we denote the thermal density of the ith component $\tilde{n}_{i,i}$ by simply $\tilde{n}_i$. The anomalous average terms $\tilde{m}_{i,j}$ are further neglected to satisfy the Hugenholtz-Pines theorem [49]. This forms the essence of the Hartree-Fock-Bogoliubov-Popov approximation. Based on these considerations and definitions, we arrive at two coupled sets of equations, one for the condensate wave functions and the second for quasiparticle amplitudes. One set of equations describing the dynamics of the condensate are the following coupled generalized GP equations:

$$i\frac{\partial\phi_{\pm 1}}{\partial t} = [\mathcal{L}_{\pm 1,\pm 1} + c_0(n_t + \tilde{n}_{\pm 1,\pm 1}) + c_2(n_{\pm 1} + n_0 - n_{\mp 1} + \tilde{n}_{\pm 1,\pm 1})]\phi_{\pm 1} + c_2\phi_0^2\phi_{\mp 1}^*$$

$$+ [(c_0 + c_2)\tilde{n}_{0,\pm 1} + 2c_2\tilde{n}_{\mp 1,0}]\phi_0 + (c_0 - c_2)\tilde{n}_{\mp 1,\pm 1}\phi_{\mp 1} - i\frac{\gamma}{\sqrt{2}}\partial_x\phi_0, \quad (4a)$$

$$i\frac{\partial\phi_0}{\partial t} = [\mathcal{L}_{0,0} + c_0(n_t + \tilde{n}_{0,0}) + c_2(n_{+1} + n_{-1})]\phi_0 + 2c_2\phi_{+1}\phi_0^*\phi_{-1} + [(c_0 + c_2)\tilde{n}_{+1,0} + 2c_2\tilde{n}_{0,-1}]\phi_{+1}$$

$$+ [(c_0 + c_2)\tilde{n}_{-1,0} + 2c_2\tilde{n}_{0,+1}]\phi_{-1} - i\frac{\gamma}{\sqrt{2}}(\partial_x\phi_{+1} + \partial_x\phi_{-1}). \quad (4b)$$

The BdG equations for quasiparticle amplitudes are given as

$$\begin{pmatrix} M_1 & -M_2 \\ M_2^* & -M_1^* \end{pmatrix}\begin{pmatrix} \mathbf{u}^\lambda \\ \mathbf{v}^\lambda \end{pmatrix} = \omega_\lambda\begin{pmatrix} \mathbf{u}^\lambda \\ \mathbf{v}^\lambda \end{pmatrix}, \quad (5)$$

where

$$M_1 = \begin{pmatrix} h_{+1,+1} + c_0 n_{+1} + c_2(2n_{+1} + n_0 - n_{-1}) & h_{+1,0} + h_{\text{SOC}} & (c_0 - c_2)(\phi_{-1}^*\phi_{+1} + \tilde{n}_{-1,+1}) \\ h_{+1,0}^* + h_{\text{SOC}} & h_{0,0} + c_0 n_0 + c_2(n_{+1} + n_{-1}) & h_{0,-1} + h_{\text{SOC}} \\ (c_0 - c_2)(\phi_{+1}^*\phi_{-1} + \tilde{n}_{+1,-1}) & h_{0,-1}^* + h_{\text{SOC}} & h_{-1,-1} + c_0 n_{-1} + c_2(n_0 - n_{+1} + 2n_{-1}) \end{pmatrix},$$

$$M_2 = \begin{pmatrix} (c_0 + c_2)\phi_{+1}^2 & (c_0 + c_2)\phi_0\phi_{+1} & (c_0 - c_2)\phi_{-1}\phi_{+1} + c_2\phi_0^2 \\ (c_0 + c_2)\phi_{+1}\phi_0 & c_0\phi_0^2 + 2c_2\phi_{+1}\phi_{-1} & (c_0 + c_2)\phi_{-1}\phi_0 \\ (c_0 - c_2)\phi_{+1}\phi_{-1} + c_2\phi_0^2 & (c_0 + c_2)\phi_0\phi_{-1} & (c_0 + c_2)\phi_{-1}^2 \end{pmatrix},$$

with

$$h_{i,j} = \left[-\frac{1}{2}\partial_x^2 - \mu + V(x) + c_0 n_t\right]\delta_{ij}, \quad h_{\text{SOC}} = \frac{-i\gamma}{\sqrt{2}}\partial_x,$$

$$h_{+1,0} = (c_0 + c_2)(\phi_0^*\phi_{+1} + \tilde{n}_{0,+1}) + 2c_2(\phi_{-1}^*\phi_0 + \tilde{n}_{-1,0}),$$

$$h_{0,-1} = (c_0 + c_2)(\phi_0\phi_{-1}^* + \tilde{n}_{-1,0}) + 2c_2(\phi_{+1}\phi_0^* + \tilde{n}_{0,+1}),$$

$$\mathbf{u}^\lambda = (u_{+1}^\lambda, u_0^\lambda, u_{-1}^\lambda)^\mathsf{T}, \quad \mathbf{v}^\lambda = (v_{+1}^\lambda, v_0^\lambda, v_{-1}^\lambda)^\mathsf{T},$$

where T denotes the transpose. The number density of the noncondensate atoms is related to the Bogoliubov quasiparticle amplitudes through

$$\tilde{n}_{i,j} = \sum_\lambda \{(u_i^{\lambda*}u_j^\lambda + v_i^\lambda v_j^{\lambda*})f_{\omega_\lambda} + v_i^\lambda v_j^{\lambda*}\}, \quad (6)$$

where $f_{\omega_\lambda} = (e^{\omega_\lambda/k_B T} - 1)^{-1}$ is the Bose factor of the λth quasiparticle state. Furthermore, the quasiparticle amplitudes are normalized as $\int \sum_i(|u_i^\lambda|^2 - |v_i^\lambda|^2)dx = 1$ and total

number of atoms is given by $N = \int n_t dx$. On diagonalizing Eq. (5), the energy of the collective excitations and the quasiparticle amplitudes are obtained. These can be used in Eq. (6) to obtain the noncondensate densities, which are eventually used in a self-consistent computation of Eqs. (4a)-(4b) and (5) to arrive at the condensate and the noncondensate densities. It should be noted that when $T \to 0$, the Bose factor $f_{\omega_\lambda} \to 0$ and $\tilde{n}_i$ reduces to $\sum_\lambda |v_i^\lambda|^2$, which accounts for the condensate depletion due to quantum fluctuations at $T = 0$. The stationary ground-state solution at $T = 0$ is numerically obtained following Refs. [50,51], which serves as an initial input for computing the noncondensate densities. Using this solution and then discretizing Eq. (5) by finite-difference methods [52], we cast Eq. (5) as a matrix eigenvalue equation and then solve it using standard matrix diagonalization algorithms to obtain the eigenenergies ω_λ and quasiparticle amplitudes u_i^λ and v_i^λ. It should be noted here that we have included the

noncondensate density terms $\tilde{n}_{i,j}$ $(i \neq j)$ in the spin channel in the above equations. These coherence terms between the thermal atoms of different components have negligible contribution in scalar BECs but become important and comparable to the spin-dependent interaction terms in the case of spinor BECs. Furthermore, if one does not include these coherence terms, the excitation spectra for two SO-coupling models, namely, $H_{\text{SOC}} = \gamma p_x f_x$ and $H'_{\text{SOC}} = \gamma p_x f_z$, which are related by a rotation about the y axis by an angle $\pi/2$, turn out to be different at finite as well as at zero temperature in the presence of quantum fluctuations. The inclusion of $\tilde{n}_{ij}$ with $i \neq j$ renders the excitation spectra for the two models equivalent, which illustrates the important role of these terms in accounting for quantum and thermal fluctuations. In fact, even in the absence of SO coupling, if these terms are not included, the excitation spectrum of a polar spin-1 BEC is not equivalent to that of an antiferromagnetic BEC with the same interaction strengths in the presence of fluctuations. In this context, it is relevant to point out that these terms were not included in several studies on spin-1 BECs based on self-consistent solutions of Eqs. (4a), (4b), and (5) [30,53].

After calculating the collective excitations, one can also compute the associated wave numbers, which essentially establishes the dispersion relation. We first compute $\tilde{u}_i^\lambda(k)$ and $\tilde{v}_i^\lambda(k)$, the Fourier transforms of the Bogoliubov quasiparticle

amplitudes $u_i^\lambda(x)$ and $v_i^\lambda(x)$, respectively, and then calculate the root-mean-square wave number k_{rms} of the λth quasiparticle mode as [43,54,55]

$$k_{\text{rms}}^\lambda = \sqrt{\frac{\sum_i \int dk \, k^2 [|\tilde{u}_i^\lambda(k)|^2 + |\tilde{v}_i^\lambda(k)|^2]}{\sum_i \int dk [|\tilde{u}_i^\lambda(k)|^2 + |\tilde{v}_i^\lambda(k)|^2]}}. \quad (7)$$

In Sec. III we will demonstrate that density and spin modes have distinct dispersion curves.

III. COLLECTIVE EXCITATIONS AT ZERO TEMPERATURE

A. Noninteracting spin-1 BEC

We first analyze the spectrum of the single-particle SO-coupled Hamiltonian

$$H_0 = \mathbb{1} \times \left[-\frac{1}{2}\partial_x^2 + \frac{x^2}{2} - \mu \right] - i\gamma f_x \partial_x, \quad (8)$$

where $\mathbb{1}$ is a 3×3 identity matrix. As H_0 and $U^\dagger H_0 U$, where U is a unitary operator, have identical spectra, we consider the $U^\dagger H_0 U$ with U defined as a rotation operator which rotates the spin state of a spin-1 particle about y by an angle $\pi/2$ in a counterclockwise direction. The unitary operator U is defined as

$$U = \begin{pmatrix} \frac{1}{2} & -\frac{1}{\sqrt{2}} & \frac{1}{2} \\ \frac{1}{\sqrt{2}} & 0 & -\frac{1}{\sqrt{2}} \\ \frac{1}{2} & \frac{1}{\sqrt{2}} & \frac{1}{2} \end{pmatrix}. \quad (9)$$

The $U^\dagger H_0 U$ thus obtained in momentum space is

$$\begin{pmatrix} -\frac{1}{2}\frac{\partial^2}{\partial k^2} + \frac{(k+\gamma)^2}{2} - \frac{\gamma^2}{2} - \mu & 0 & 0 \\ 0 & -\frac{1}{2}\frac{\partial^2}{\partial k^2} + \frac{k^2}{2} - \mu & 0 \\ 0 & 0 & -\frac{1}{2}\frac{\partial^2}{\partial k^2} + \frac{(k-\gamma)^2}{2} - \frac{\gamma^2}{2} - \mu \end{pmatrix},$$

with eigenfunctions

$$\begin{pmatrix} \frac{1}{\sqrt{2^n\sqrt{\pi}n!}} \exp\left(\frac{-(k+\gamma)^2}{2}\right)H_n(k) \\ 0 \\ 0 \end{pmatrix}, \quad \begin{pmatrix} 0 \\ \frac{1}{\sqrt{2^n\sqrt{\pi}n!}} \exp\left(\frac{-k^2}{2}\right)H_n(k) \\ 0 \end{pmatrix}, \quad \begin{pmatrix} 0 \\ 0 \\ \frac{1}{\sqrt{2^n\sqrt{\pi}n!}} \exp\left(\frac{-(k-\gamma)^2}{2}\right)H_n(k) \end{pmatrix} \quad (10)$$

and eigenspectrum

$$\epsilon_{\pm 1}(n) = \left(n + \frac{1}{2}\right) - \frac{\gamma^2}{2} - \mu, \quad \epsilon_0(n) = \left(n + \frac{1}{2}\right) - \mu, \quad (11)$$

where $n = 0, 1, 2, \ldots$, $\mu = (1 - \gamma^2)/2$, and $H_n(k)$ is the Fourier transform of the nth-order Hermite polynomial. So we get two degenerate eigenfunctions and the third is shifted up by $\gamma^2/2$ for each value n. In the absence of a trap, the energy dispersion is

$$\epsilon_{\pm 1}(k) = \frac{(k \pm \gamma)^2}{2} - \frac{\gamma^2}{2} - \mu, \quad \epsilon_0(k) = \frac{k^2}{2} - \mu, \quad (12)$$

where μ would be fixed by the number density. The effect of SO coupling is therefore to open a gap and also shift the minima of $\epsilon_{\pm 1}$ with respect to ϵ_0. The eigenfunctions of H_0 corresponding to eigenenergies $\epsilon_{\pm 1}(n)$ and $\epsilon_0(n)$ are, respectively,

$$\frac{1}{\sqrt{2^n\sqrt{\pi}n!}} \exp(-\{x/2 \pm i\gamma\}x)H_n(x) \begin{pmatrix} \frac{1}{2} \\ \pm\frac{1}{\sqrt{2}} \\ \frac{1}{2} \end{pmatrix}, \quad (13)$$

$$\frac{1}{\sqrt{2^n\sqrt{\pi}n!}} \exp(-x^2/2)H_n(x) \begin{pmatrix} -\frac{1}{\sqrt{2}} \\ 0 \\ \frac{1}{\sqrt{2}} \end{pmatrix}. \quad (14)$$
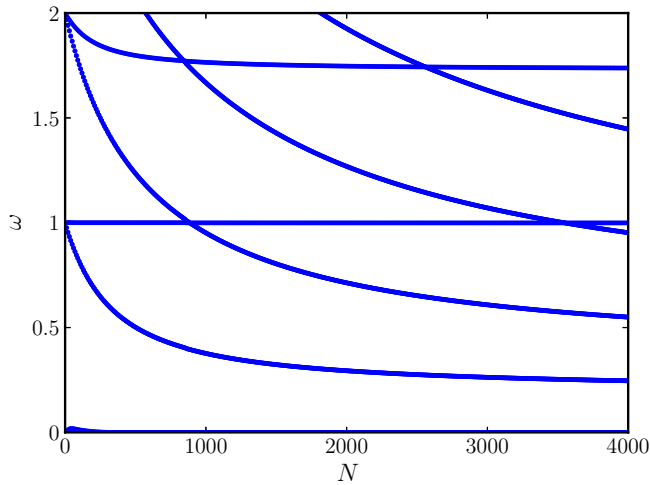
FIG. 1. Low-lying excitation spectrum for the ^{23}Na spin-1 BEC with $c_0 = 0.0119N$, $c_2 = 0.000\,424N$, and $\gamma = 0$ as a function of the number of atoms N at zero temperature. Each set of three degenerate modes in the noninteracting limit splits into two branches in the presence of interactions: The low-lying branch consists of two degenerate spin modes and the other corresponds to a single density mode.

FIG. 2. Excitation spectrum for the ^{23}Na spin-1 BEC with $c_0 = 0.0119N$, $c_2 = 0.000\,424N$, and $\gamma = 0.5$ as a function of the number of atoms N at zero temperature. The two degenerate modes in the noninteracting limit bifurcate with the energy of the spin mode (marked with red stars), becoming lower than the corresponding density mode (marked with black triangles).

B. Interacting spin-1 BEC without SO coupling

We now discuss the role of contact interactions on the ground state of spin-1 spinor condensates at $T = 0$ K and associated excitation spectra in the absence of spin-orbit coupling and quantum fluctuations. In particular, as a representative example, we consider the antiferromagnetic phase of ^{23}Na [1] atoms in the $F = 1$ manifold confined in a cigar-shaped trapping potential with the trapping parameters $\omega_x = 2\pi \times 5$ Hz and $\omega_y = \omega_z = 20\omega_x$ and having scattering lengths $a_0 = 48.91a_B$ and $a_2 = 54.54a_B$ [56], where a_B is the Bohr radius. The interaction strengths, in dimensionless units, translate to $c_0 = 0.0119N$ and $c_2 = 0.000\,424N$. With an increase in the number of atoms, the spatial extent of the ground-state density profiles increases. The antiferromagnetic order constrains zero population in the $m_f = 0$ hyperfine state but with an equal population in the $m_f = 1$ and -1 states or all the atoms in the $m_f = 0$ state. The longitudinal magnetization $M_z = \int dx(|\phi_{+1}|^2 - |\phi_{-1}|^2)$ is hence equal to zero. We further investigate the excitation spectrum of the antiferromagnetic phase which is accomplished by diagonalizing the BdG matrix in (5). In Fig. 1 we show the variation in the excitation frequencies with the total number of atoms N. For a single particle, i.e., when the interactions are absent, the excitation spectrum is exactly equivalent to the spectra of three independent harmonic oscillators. However, in the presence of interactions, the equations get coupled. Here the spectrum is characterized by the three Goldstone modes with zero excitation frequency. These modes also serve as a self-consistency check for the accuracy of our numerical calculations. The presence of three Goldstone modes is attributed to the fact that for the antiferromagnetic phase, the symmetry group is U(1) $\times$ S^2 [44] such that we can have three broken symmetries. Apart from the one *density* Goldstone mode arising out of the breaking of U(1) gauge symmetry, the other two *spin* Goldstone modes emanate from
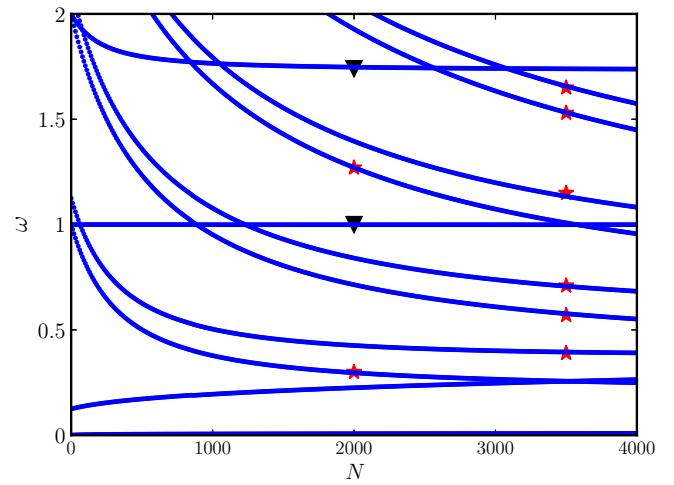
the breaking of two symmetry generators of the spin rotation [57]. Among the nonzero low-lying modes, with introduction of the interactions, the degeneracy between the modes with $\omega = 1$ is lifted with a bifurcation into two branches. One branch corresponds to the density-dipole mode whose energy remains constant with increasing N satisfying Kohn's theorem [58]. The other branch consists of two degenerate spin-dipole modes. At the outset with an increase in N, the energy of these spin modes decreases sharply and then gets saturated for higher values of N. Similarly, three degenerate modes with $\omega = n$ for a noninteracting system where $n = 2, 3, \ldots$ lead to two degenerate spin modes and a density mode having energy higher than that of the corresponding spin modes with the introduction of interactions as shown in Fig. 1.

C. Interacting spin-1 BEC with SO coupling

In Fig. 2 we show the variation in the excitation frequencies as a function of the total number of atoms N with fixed SO coupling strength ($\gamma = 0.5$). The excitation spectrum is characterized by two zero-energy modes which are identified as two Goldstone modes. One of these is a density Goldstone mode arising out of the breaking of U(1) gauge symmetry and the other is a spin Goldstone mode originating from the breaking of global SO(2) spin-space rotation symmetry [14]. For a small number of atoms, the first nonzero mode is shifted approximately by $\gamma^2/2$ as shown in Fig. 2. Among the nonzero low-lying modes, in the presence of SO coupling, is the density-dipole mode, with frequency $\omega = 1$, which remains constant with increasing N satisfying Kohn's theorem. Another consequence of SO coupling is the lifting of the degeneracy between two spin modes as can be seen by comparing Figs. 1 and 2. On increasing the interaction strengths, the energy of these nondegenerate spin modes decreases and then gets saturated for higher values of N. The energy separation between these two spin modes remains approximately
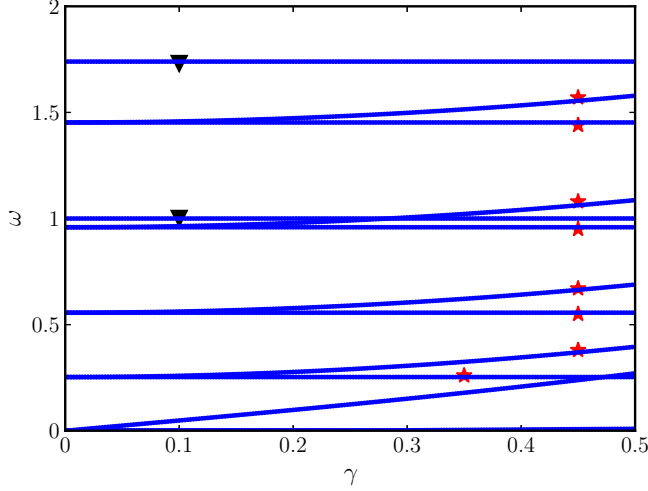
FIG. 3. Excitation spectrum for the ^{23}Na spin-1 BEC with $c_0 = 0.0119N$, $c_2 = 0.000\,424N$, and $N = 4000$ as a function of SO coupling strength γ at zero temperature. The modes bifurcating from $\gamma = 0$ are the spin modes (marked with red stars), whereas the remaining modes not changing with a variation in γ are density modes (marked with black triangles).

equal to $\gamma^2/2$ with a variation in the number of atoms. As expected, for a fixed value of N, increasing γ increases the energy of one of the spin modes in the pair, whereas the energy of the other spin and density modes remains unchanged. This is demonstrated in Fig. 3, where the excitation spectrum is plotted as a function of SO-coupling strength. The modes which are bifurcating from $\gamma = 0$ in Fig. 3 are the spin modes, while the remaining modes are the density modes.

To further understand the role of SO coupling in the excitation spectrum, we consider $H'_{\text{SOC}} = \gamma p_x f_z$, where the absence of the $m_f = 0$ component as shown in Fig. 4(a) at $T = 0$ K results in the decoupling of the BdG equations (5) corresponding to quasiparticle amplitudes $(u^\lambda_{\pm 1}, v^\lambda_{\pm 1})$ from those for $(u^\lambda_0, v^\lambda_0)$. On the other hand, for $H_{\text{SOC}} = \gamma p_x f_x$ all $m_f = 0, \pm 1$ components are nonzero, as shown in Fig. 4(b) [14]. The solution shown in Fig. 4(b) can be obtained by operating U in Eq. (9) on the solution shown in Fig. 4(a). The resultant
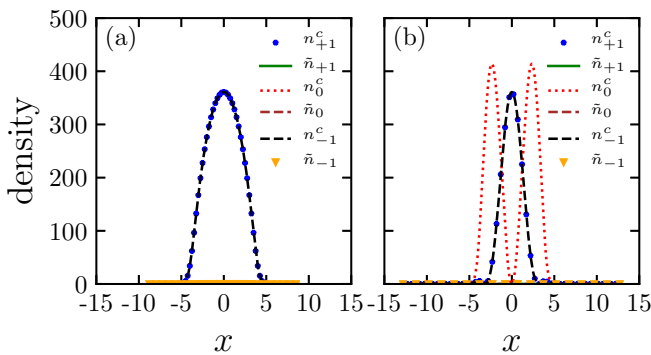

FIG. 4. (a) Condensate densities $n_i^c(x)$ and thermal densities $\tilde{n}_i(x)$ for the ^{23}Na spin-1 BEC with $c_0 = 0.0119N$, $c_2 = 0.000\,424N$, $N = 4000$, $\gamma = 0.5$, and SO coupling $H'_{\text{SOC}} = \gamma f_z p_x$. (b) Same as in (a) but for $H_{\text{SOC}} = \gamma f_x p_x$.

eigenvalue equation for $(u^\lambda_{\pm 1}, v^\lambda_{\pm 1})$ with $H'_{\text{SOC}} = \gamma p_x f_z$ is

$$
\begin{pmatrix} A + i\gamma\,\partial_x & -B & C & -D \\ B^* & -A + i\gamma\,\partial_x & D^* & C^* \\ C^* & -D & E - i\gamma\,\partial_x & -F \\ D^* & -C & F^* & -E - i\gamma\,\partial_x \end{pmatrix}
$$

$$
\times \begin{pmatrix} u^\lambda_{+1} \\ v^\lambda_{+1} \\ u^\lambda_{-1} \\ v^\lambda_{-1} \end{pmatrix} = \omega_{\pm\lambda} \begin{pmatrix} u^\lambda_{+1} \\ v^\lambda_{+1} \\ u^\lambda_{-1} \\ v^\lambda_{-1} \end{pmatrix}, \tag{15}
$$

where

$$
A = \left[-\tfrac{1}{2}\partial_x^2 - \mu + V(x) \right] + 2(c_0 + c_2)n^c_{+1}
$$
$$
+ (c_0 - c_2)n^c_{-1}, \quad B = (c_0 + c_2)\phi^2_{+1},
$$
$$
C = (c_0 - c_2)\phi_{+1}\phi^*_{-1}, \quad D = (c_0 - c_2)\phi_{+1}\phi_{-1},
$$
$$
E = \left[-\tfrac{1}{2}\partial_x^2 - \mu + V(x) \right] + 2(c_0 + c_2)n^c_{-1}
$$
$$
+ (c_0 - c_2)n^c_{+1}, \quad F = (c_0 + c_2)\phi^2_{-1}.
$$

and that for $(u^\lambda_0, v^\lambda_0)$ is

$$
\begin{pmatrix} R & -S \\ S^* & -R \end{pmatrix} \begin{pmatrix} u^\lambda_0 \\ v^\lambda_0 \end{pmatrix} = \omega_{0\lambda} \begin{pmatrix} u^\lambda_0 \\ v^\lambda_0 \end{pmatrix}, \tag{16}
$$

where $R = [-\partial_x^2/2 - \mu + V(x)] + (c_0 + c_2)(n^c_{+1} + n^c_{-1})$ and $S = 2c_2\phi_{+1}\phi_{-1}$. Equation (15) is the same as the BdG equations of a pseudospinor-$\frac{1}{2}$ BEC consisting of $m_f = \pm 1$ components with an SO coupling of $\gamma p_x \sigma_z$, where σ_z is a Pauli spin matrix for the spin-$\frac{1}{2}$ system. Moreover, the eigenmodes in (16) are shifted upward by $\gamma^2/2$ compared to the spin mode in (15). As mentioned earlier, spin-1 BECs with H_{SOC} and H'_{SOC} have identical spectra; the quasiparticle amplitudes with the former can be obtained from a unitary transformation, defined by U in (9), of the quasiparticle amplitudes for the latter. In Sec. III E we use the variational method to calculate a few low-lying modes corresponding to Eq. (15).

To understand the breakdown in the degeneracy between the pairs of spin modes in the presence of SO coupling, we analyze their Bogoliubov amplitudes and phases. As an example in Figs. 5(a) and 5(b), the Bogoliubov amplitudes of the two spin-dipole modes for $c_0 = 0.0119N$ and $c_2 = 0.000\,424N$ with $N = 4000$ are plotted. The $|u_i|$ and $|v_i|$ for the two modes are identical without and with $\gamma f_z p_x$ SO coupling. The excitation frequencies of the modes with $\gamma = 0$ and 0.5 were already shown in Figs. 1 and 2, respectively. The phase profiles corresponding to the Bogoliubov amplitudes in Figs. 5(a) and 5(b) with $\gamma = 0$ are shown in Figs. 6(a) and 6(b), respectively, and the same with $H'_{\text{SOC}} = 0.5f_z p_x$ are shown in Figs. 6(c) and 6(d), respectively. With SO coupling the mode with lower excitation frequency acquires an SO-coupling strength-dependent phase gradient, whereas the phase profile of the mode with higher excitation frequency remains unchanged. Without SO coupling these Bogoliubov modes can be transformed from one to another by a rotation in spin space about the y axis by an angle $\pi/2$, whereas in the presence of SO coupling the modes are not connected by such a unitary transformation. The breakdown in degeneracy of the spin-dipole modes is also accompanied by distinct spin-density vectors $(\mathbf{f} = \langle f_x \rangle, \langle f_y \rangle, \langle f_z \rangle)$ as shown in
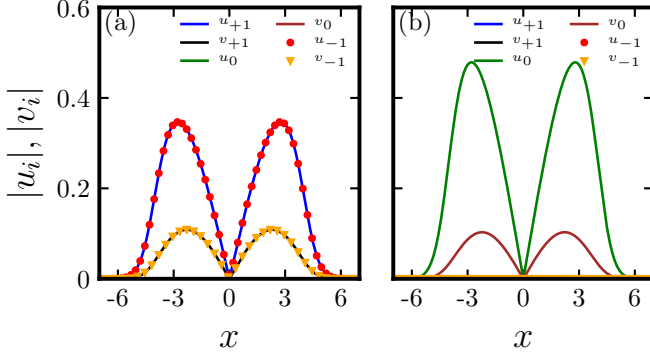
FIG. 5. Bogoliubov amplitudes for the spin-dipole modes with $c_0 = 0.0119N$, $c_2 = 0.000\,424N$, and $N = 4000$. Without SO coupling, (a) and (b) show $|u_i|$ and $|v_i|$ for two degenerate spin-dipole modes. These are also identical to the spin-dipole modes in the presence of $H'_{\mathrm{SOC}} = 0.5 f_z p_x$, where (a) and (b) are equivalent to the amplitudes for the spin-dipole modes with lower and higher frequency, respectively.

Figs. 6(e) and 6(f) for lower- and higher-frequency spin modes, respectively.

We have also numerically computed the dispersion curves for the system as shown in Fig. 7. For the spin-1 BEC, the spin-independent interaction strength is higher than the spin-dependent interaction strength, making the energy of density excitations greater than the spin excitations for any given k_{rms} as shown in Fig. 7(a) in the absence of SO coupling. In Fig. 7(a) the dispersions for the two spin modes overlap, indicating the degeneracy between the modes. Furthermore, the presence of SO coupling lifts the degeneracy between these modes, as is shown in Fig. 7(b). The dispersions in the
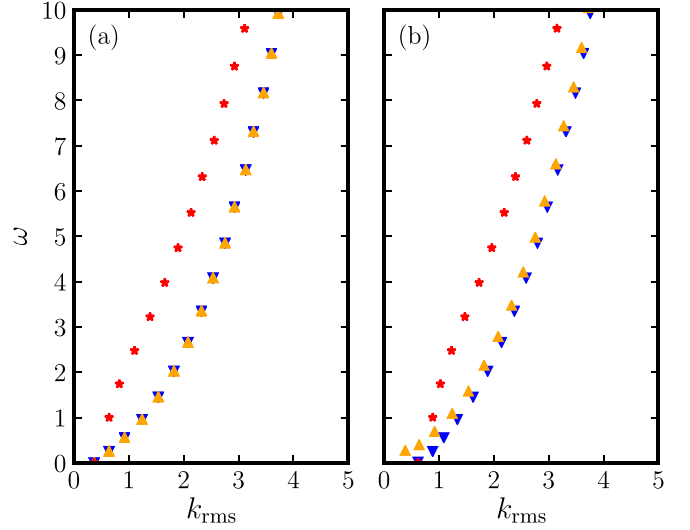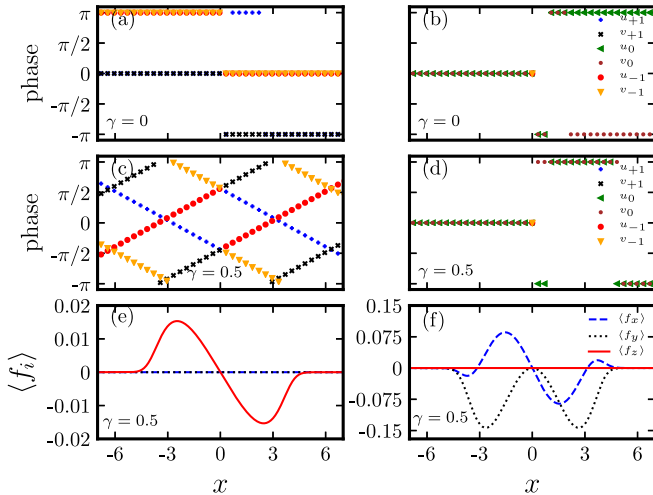

FIG. 6. (a) and (b) Phase profiles of the spin-dipole modes in the absence of SO coupling corresponding to the Bogoliubov amplitudes shown in Figs. 5(a) and 5(b), respectively. (c) and (d) Corresponding phase profiles with $H'_{\mathrm{SOC}} = 0.5 f_z p_x$ of the lower- and higher-frequency spin-dipole modes. (e) and (f) Spin textures corresponding to the lower- and higher-frequency spin-dipole modes in the presence of $H'_{\mathrm{SOC}} = 0.5 f_z p_x$. Here $\langle \ldots \rangle$ represents the expectation with respect to the perturbed order parameter.

FIG. 7. (a) Dispersion curves of the ^{23}Na spin-1 BEC with $c_0 = 0.0119N$, $c_2 = 0.000\,424N$, $N = 4000$, and $\gamma = 0$. (b) Same as (a) but for $\gamma = 0.5$. Red stars represent the dispersion for the density modes, whereas up- and down-pointing triangles correspond to dispersion for spin modes. The lifting of degeneracy between the spin modes in the presence of SO coupling results in three distinct dispersion branches in (b).

presence and absence of SO coupling are consistent with the excitation spectra in Figs. 1 and 2, respectively.

D. Dynamics

In order to examine the nature of the low-lying collective excitations through physical observables and validate our theoretical predictions of mode frequencies obtained from the BdG equations, we perform direct numerical dynamical real-time simulations of the system by evolving the ground state with appropriate perturbations. The time evolution is done using $T = 0$ K coupled GP equations. This type of procedure has already been used experimentally to study low-lying collective excitations by modulating the trapping potential for density [21] and spin-dipole modes [59]. We, however, use perturbation by constructing the fluctuation operator corresponding to the dipole and breathing modes in the density and spin channels. The fluctuation is constructed with the Bogoliubov quasiparticle amplitudes u and v corresponding to the frequency ω of the relevant mode. To execute, we add the fluctuation $\delta \psi_i \propto u_i^\lambda - v_i^{*\lambda}$ to the ground-state wave function at time $t = 0$ to excite a mode with frequency ω_λ. The system is then evolved and a relevant physical observable is monitored over time. We consider the ^{23}Na spin-1 BEC consisting of 4000 atoms with $c_0 = 0.0119N$, $c_2 = 0.000\,434N$, and a SO coupling $H'_{\mathrm{SOC}} = \gamma p_x f_z$, where $\gamma = 0.5$ in the remainder of this section.

1. Density-dipole and breathing modes

To excite the density-dipole mode, we study the center-of-mass motion via $x_{\mathrm{c.m.}}(t) = \langle x \rangle = \sum_{i=-1,0,+1} \int x |\phi_i(x, t)|^2 dx$, where $\langle \ldots \rangle$ corresponds to an expectation with respect to the time-evolved ground state. In Fig. 8(a) we plot the time
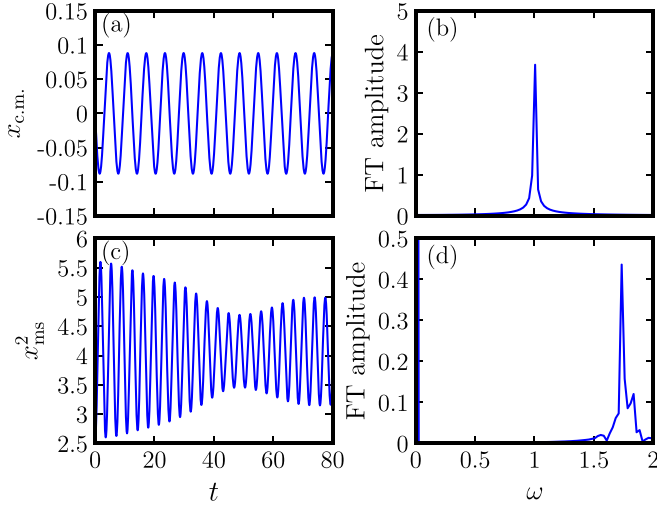
FIG. 8. (a) Center-of-mass oscillations, i.e., $x_{c.m.}(t)$, as a function of time and (b) the Fourier transform of $x_{c.m.}(t)$ with a dominant peak at $\omega = 1$. Similarly, (c) shows the oscillations in the mean-square size of the system $x_{ms}^2(t)$ and (d) the Fourier transform of $x_{ms}^2(t)$ with a dominant peak at $\omega = 1.73$. The dynamics corresponds to the ^{23}Na spin-1 BEC consisting of 4000 atoms with $c_0 = 0.0119N$, $c_2 = 0.000\,424N$, and $\gamma = 0.5$. Both (a) and (c) represent the density excitations.

dependence of $x_{c.m.}(t)$. We compute the Fourier transform (FT) of $x_{c.m.}(t)$ to demonstrate that the dominant frequency resonates at $\omega = 1$; the FT is shown in Fig. 8(b). Experimentally, the density-dipole mode is excited by a translational shift in the external trapping potential [21]. Furthermore, to examine the excitation of the breathing mode, we consider the corresponding observable x^2 and calculate the mean-square radius $x_{ms}^2(t) = \langle x^2 \rangle = \sum_{i=-1,0,+1} \int x^2 |\phi_i(x,t)|^2 dx$ as a function of time. In Figs. 8(c) and 8(d) we show the variation in $x_{ms}^2(t)$ and the most dominant peak at $\omega = 1.73$ in the FT of $x_{ms}^2(t)$. The density-breathing mode can also be excited by perturbing the trap strength [21]. It is worth mentioning here that the frequency of oscillations obtained from the real-time dynamics indeed agrees quite well with the corresponding collective excitations obtained from the equilibrium BdG analysis as shown in Fig. 2 for $N = 4000$ and $\gamma = 0.5$.

2. Spin-dipole and spin-breathing modes

We now turn our attention to excite the spin channel where we first choose the observable $x f_z$ which corresponds to the spin-dipole mode. We study the dynamics of $d_x(t) = \langle x f_z \rangle = \int \phi_i^*(x,t)(x f_z)_{ij}\phi_j(x,t)dx = \sum_{i=-1,1} \int x |\phi_i(x,t)|^2 dx$. In Fig. 9(a) we plot the time dependence of d_x and in Fig. 9(b) the frequency dependence of the FT of d_x with a primary peak at $\omega = 0.25$. Similarly, the spin-breathing mode corresponds to the observable $x^2 f_z$. In Figs. 9(c) and 9(d) we show the dynamics of $d_x^2 = \langle x^2 f_z \rangle = \sum_{i=-1,1} \int x^2 |\phi_i(x,t)|^2 dx$, i.e., the relative difference in the mean-square radii of the $m_f = \pm 1$ components and the associated FT with a dominant peak at $\omega = 0.55$, respectively. The frequencies of oscillations thus obtained from the dynamics conform to the BdG analysis of the antiferromagnetic
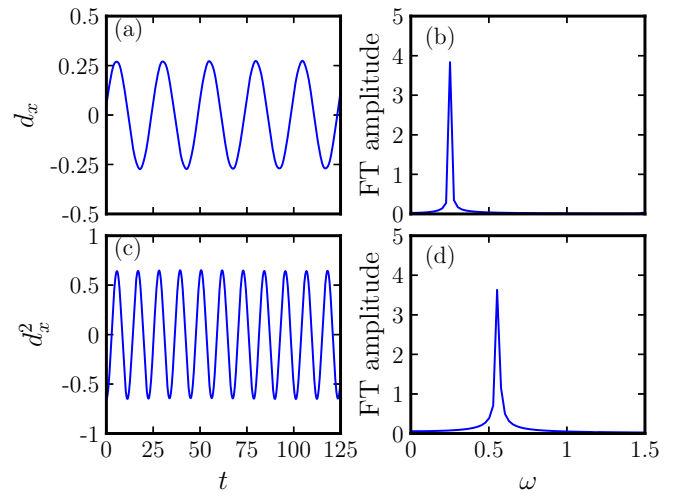

FIG. 9. Plots showing (a) $d_x(t) = \langle x f_z \rangle$ as a function of time and (b) the Fourier transform of $d_x(t)$ with a dominant peak at $\omega = 0.25$. (c) and (d) Same as (a) and (b) but for $d_x^2(t) = \langle x^2 f_z \rangle$ and its Fourier transform with a dominant peak at $\omega = 0.55$, respectively. The peaks in (b) and (d) are the frequencies of spin-dipole and spin-breathing modes, respectively. The dynamics corresponds to the ^{23}Na spin-1 BEC consisting of 4000 atoms with $c_0 = 0.0119N$, $c_2 = 0.000\,424N$, and $\gamma = 0.5$. Both (a) and (c) represent the spin excitations.

spinor condensates at equilibrium, as illustrated in Fig. 2 for $N = 4000$ and $\gamma = 0.5$.

3. Shifted spin-dipole and spin-breathing modes

We now discuss the excitation of the spin modes whose energies increase with an increase in SO-coupling strength as discussed in Sec. III C. As mentioned earlier, these are precisely the modes appearing in Eq. (16). Here we first consider the observable $x f_x$ corresponding to the shifted spin-dipole (SSD) mode and study the time dependence of its expectation, i.e., $l_x(t) = \int \phi_i^*(x,t)(x f_x)_{ij}\phi_j(x,t)dx$. We show $l_x(t)$ as a function of t and the frequency dependence of its FT with a primary peak at $\omega = 0.395$ in Figs. 10(a) and 10(b), respectively. Similarly, the shifted spin-breathing (SSB) mode corresponds to the observable $x^2 f_x$. In Figs. 10(c) and 10(d) we illustrate the dynamics of $l_x^2(t) = \langle x^2 f_x \rangle = \int \phi_i^*(x,t)(x^2 f_x)_{ij}\phi_j(x,t)dx$ and the corresponding FT with a dominant peak at $\omega = 0.685$, respectively. The frequencies of oscillations thus obtained from the dynamics, i.e., 0.395 and 0.685 for SSD and SSB modes, respectively, agree very well with the BdG analysis of the antiferromagnetic spinor condensates at equilibrium, as illustrated in Fig. 2 for $N = 4000$ and $\gamma = 0.5$.

All of these modes can also be excited for $H_{SOC} = \gamma p_x f_x$ with exactly the same excitation frequencies. The relevant observable in this case can be obtained by a transformation $U\hat{O}U^\dagger$, where $\hat{O}$ is the observable for $H'_{SOC} = \gamma p_x f_z$. This implies that with H_{SOC}, the observable for the density modes will remain the same, i.e., x and x^2 for density-dipole and density-breathing modes, respectively. On the other hand, the observables for spin-dipole and spin-breathing modes are $x f_x$ and $x^2 f_x$, respectively, while for the shifted spin-dipole
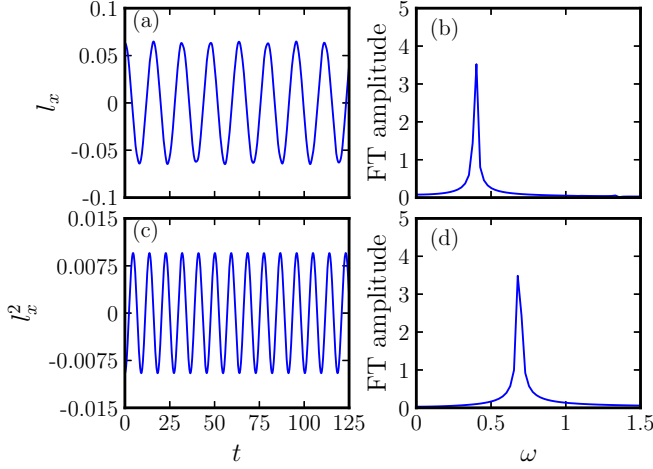
FIG. 10. Plots showing (a) $l_x(t) = \langle x f_x \rangle$ as a function of time and (b) the Fourier transform of $l_x(t)$ with a dominant peak at $\omega = 0.395$. (c) and (d) Same as (a) and (b) but for $l_x^2(t) = \langle x^2 f_x \rangle$ and its Fourier transform with a dominant peak at $\omega = 0.685$, respectively. The peaks in (b) and (d) are the frequencies of SSD and SSB modes, respectively. The dynamics corresponds to the ^{23}Na spin-1 BEC consisting of 4000 atoms with $c_0 = 0.0119N$, $c_2 = 0.000\,424N$, and $\gamma = 0.5$. Both (a) and (c) represent the spin excitations.

and spin-breathing modes, the operators are $x f_z$ and $x^2 f_z$, respectively.

E. Variational analysis

For a quasi-one-dimensional spin-1 BEC, the spectrum of the low-energy excitations can be studied by using a time-dependent variational method introduced in Refs. [60,61]. For simplicity, we have considered $H'_{SOC} = \gamma p_x f_z$, which, as discussed earlier, allows the spectrum analysis as a composition of the spectra of two subsystems: one of which corresponds to a pseudospin-$\frac{1}{2}$ BEC of $m_f = \pm 1$ components with $\gamma p_x \sigma_z$ SO coupling and the second corresponding to the excitation in the $m_f = 0$ component of the SO-coupled spin-1 BEC. We calculate a few low-lying modes of the pseudospinor subsystem using the variational method. We consider the Gaussian variational ansatz

$$\phi_{\pm 1}(x, t) = A(t) \exp \left[-\frac{\{x - x_{\pm 1}(t)\}^2}{2\sigma(t)^2} + i\alpha_{\pm 1}(t) \right.$$

$$\left. \times \{x - x_{\pm 1}(t)\} + i\beta(t)\{x - x_{\pm 1}(t)\}^2 \right], \quad (17)$$

where σ, $x_{\pm 1}$, $\alpha_{\pm 1}$, and β, which denote the condensate width, displacement of the $m_f = \pm 1$ components from the center of a harmonic trap, phase gradient, and chirp, respectively, are the time-dependent variational parameters. The Lagrangian of the subsystem is

$$L = \int \sum_{j=-1,+1} dx \frac{i}{2} \left(\phi_j^* \frac{\partial \phi_j}{\partial t} - \phi_j \frac{\partial \phi_j^*}{\partial t} \right) - E, \quad (18)$$

where the energy E is defined as

$$E = N \int_{-\infty}^{\infty} \left\{ \sum_{j=-1,+1} \left(\frac{1}{2} \left| \frac{d\phi_j}{dx} \right|^2 + V n_j^c \right) \right.$$

$$+ \frac{c_0}{2} \left(n_{+1}^c + n_{-1}^c \right)^2 + \frac{c_2}{2} \left(n_{+1}^c - n_{-1}^c \right) n_{+1}^c$$

$$+ \frac{c_2}{2} \left(n_{-1}^c - n_{+1}^c \right) n_{-1}^c$$

$$\left. + \gamma \left(-i\phi_{+1}^* \frac{d\phi_{+1}}{dx} + i\phi_{-1}^* \frac{d\phi_{-1}}{dx} \right) \right\} dx. \quad (19)$$

We insert Eq. (17) in Eq. (18) and then compute the Euler-Lagrange equations. The Euler-Lagrange equations for the phase gradients are $\alpha_{\pm 1} = m\dot{x}_{\pm 1}/\hbar$ and for the chirp $\beta = \dot{\sigma}/2\sigma$, which are then used in the equation of motion for $x_{\pm 1}$ and the condensate width σ, respectively. After linearizing the resultant Euler equations, we get the equations of motion

$$\delta\ddot{\sigma}(t) + \delta\sigma(t) = -\sqrt{\frac{2}{\pi}} \frac{c_0}{\sigma^3} \delta\sigma(t) - \frac{3}{\sigma^4} \delta\sigma(t)$$

$$+ \frac{\sqrt{2}}{\pi} \frac{c_0 - c_2}{\sigma^5} (x_{+1} - x_{-1})^2 \delta\sigma(t)$$

$$- \frac{1}{\sqrt{2\pi}} \frac{c_0 - c_2}{\sigma^4} (x_{+1} - x_{-1})$$

$$\times [\delta x_{+1}(t) - \delta x_{-1}(t)], \quad (20a)$$

$$\delta\ddot{x}_{+1}(t) + \delta x_{+1}(t) = \frac{1}{2\sqrt{2\pi}} \frac{c_0 - c_2}{\sigma^3} [\delta x_{+1}(t) - \delta x_{-1}(t)]$$

$$- \frac{3}{2\sqrt{2\pi}} \frac{c_0 - c_2}{\sigma^4} \delta\sigma(t)(x_{+1} - x_{-1}), \quad (20b)$$

$$\delta\ddot{x}_{-1}(t) + \delta x_{-1}(t) = -\frac{1}{2\sqrt{2\pi}} \frac{c_0 - c_2}{\sigma^3} [\delta x_{+1}(t) - \delta x_{-1}(t)]$$

$$+ \frac{3}{2\sqrt{2\pi}} \frac{c_0 - c_2}{\sigma^4} \delta\sigma(t)(x_{+1} - x_{-1}), \quad (20c)$$

where σ and $x_{\pm 1}$ are to be understood as the equilibrium values. For breathing oscillation, we consider $\delta x_{\pm 1}(t) = 0$. The equation of motion from (19) for the condensate width σ results in

$$\delta\ddot{\sigma}(t) + \left(1 + \frac{3}{\sigma^4} + \sqrt{\frac{2}{\pi}} \frac{c_0}{\sigma^3} \right) \delta\sigma(t) = 0. \quad (21)$$

The equilibrium width σ of the condensate satisfies

$$\sigma^4 - \frac{c_0 \sigma}{\sqrt{2\pi}} = 1 \quad (22)$$

and the eigenfrequency of the oscillations in the width about its equilibrium value is

$$\omega_b = \left[1 + \frac{3}{\sigma^4} + \sqrt{\frac{2}{\pi}} \frac{c_0}{\sigma^3} \right]^{1/2}, \quad (23)$$

which is equal to 1.737 for $c_0 = 0.0119N$ with $N = 4000$. The variational result matches with the density-breathing mode

of the BdG spectrum shown in Fig. 2. For dipole and spin-dipole oscillation, we consider $\delta\sigma(t) = 0$ and add and subtract Eqs. (20b) and (20c) to obtain the equations of motion

$$[\delta\ddot{x}_{+1}(t) + \delta\ddot{x}_{-1}(t)] + [\delta x_{+1}(t) + \delta x_{-1}(t)] = 0, \quad (24a)$$

$$[\delta\ddot{x}_{+1}(t) - \delta\ddot{x}_{-1}(t)] + [\delta x_{+1}(t) - \delta x_{-1}(t)]$$

$$= \frac{1}{\sqrt{2\pi}} \frac{c_0 - c_2}{\sigma^3} [\delta x_{+1}(t) - \delta x_{-1}(t)]. \quad (24b)$$

In terms of the center-of-mass coordinate $\delta x_1(t) + \delta x_{-1}(t)$ and relative coordinate $\delta x_1(t) - \delta x_{-1}(t)$, Eq. (24a) corresponds to the center-of-mass motion oscillating with trap frequency $\omega = 1$ satisfying Kohn's theorem and Eq. (24b) corresponds to the frequency

$$\omega_{sd} = \sqrt{1 - \sqrt{\frac{1}{2\pi} \frac{c_0 - c_2}{\sigma^3}}} \quad (25)$$

of the spin-dipole mode. For $c_0 = 0.0119N$ and $c_2 = 0.000\,424N$ with $N = 4000$, we get $\omega_{sd} = 0.23$, which is very close to the spin-dipole frequency 0.25 calculated from the BdG analysis shown in Fig. 2. Equations (24a) and (24b) also indicate that in the presence of a harmonic trap, the center-of-mass and relative motions are decoupled.

IV. COLLECTIVE EXCITATIONS AT FINITE TEMPERATURE

We now analyze the excitation spectra of the SO-coupled ^{23}Na spin-1 BEC with $c_0 = 0.0119N$, $c_2 = 0.000\,424N$, and $\gamma = 0.5$ at finite temperatures and consisting of $N = 2000$ and 4000. The excitation spectrum is calculated by solving Eqs. (4a), (4b), and (5) self-consistently with the noncondensate density computed from Eq. (6). As an example of static density profiles, the condensate and the noncondensate densities of the system with $N = 4000$ are shown in Fig. 11 at $T = 0.2T_c$ and $0.4T_c$, where $T_c = 40.56$ nK is the critical temperature for an ideal spin-1 Bose gas in a quasi-one-dimensional harmonic trap [62–64]. In Figs. 11(a) and 11(b) we show the density profiles with $H_{\mathrm{SOC}} = \gamma p_x f_x$, and in Figs. 11(c) and 11(d) the same but with $H'_{\mathrm{SOC}} = \gamma p_x f_z$. With increasing temperature, the number of thermal atoms increases along with the spatial extent of the thermal cloud. This is accompanied by a corresponding decrease in the condensate density. The repulsive interaction between the condensate and noncondensate clouds results in a dip in the noncondensate density at the center of the trap and emergence of density peaks towards the edges of the trap as shown in Figs. 11(a)–11(d). In Figs. 12(a) and 12(b) we show the excitation spectra of nonzero modes as a function of temperature in the presence of SO coupling for $N = 2000$ and 4000, respectively. With an increase in temperature, the density and the spin modes show qualitatively distinct behavior. We observe that the frequencies of density modes decrease with an increase in temperature, whereas those of spin modes increase with the temperature. The behavior of density modes can be understood by the fact that at higher temperatures, the excitations are those of a condensate in an effective potential and that the effective potential is weakened [65] by the presence of the static thermal cloud, thus lowering the harmonic potential
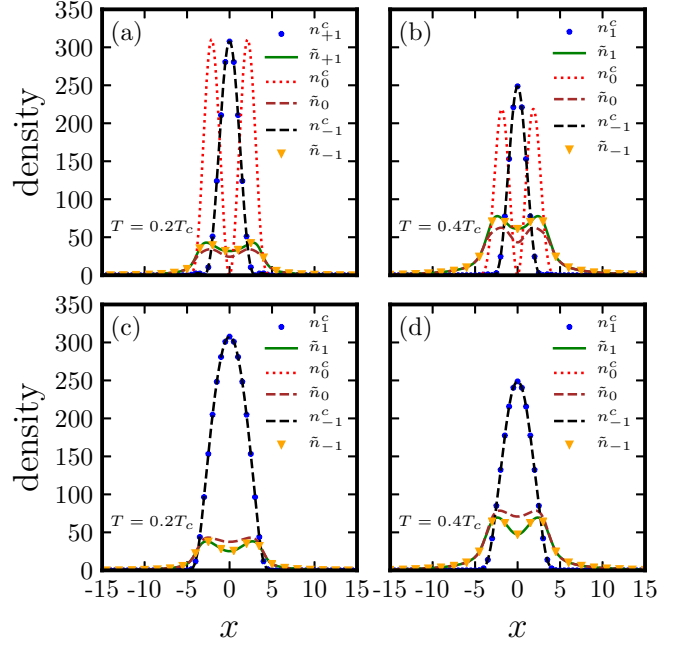

FIG. 11. Condensate densities $n_i^c(x)$ and thermal densities $\tilde{n}_i(x)$ for the ^{23}Na spin-1 BEC with $c_0 = 0.001\,19N$, $c_2 = 0.000\,424N$, $N = 4000$, $\gamma = 0.5$, and $H_{\mathrm{SOC}} = \gamma f_x p_x$ at (a) $T = 0.2T_c$ and (b) $T = 0.4T_c$. (c) and (d) Same as (a) and (b) but for $H'_{\mathrm{SOC}} = \gamma f_z p_x$ at $T = 0.2T_c$ and $0.4T_c$, respectively.

and thereby decreasing the frequency. On the other hand, the increasing of the spin modes' frequencies can be understood by the fact that at finite temperature, the numbers of atoms in the condensates are decreasing, so by using an equivalent zero-temperature condensate [66] solution, we get qualitatively the same behavior for spin modes as shown in Fig. 12. It should be noted from Fig. 2 that for $N \geqslant 2000$ the spin modes are much more sensitive to a change in the number of atoms in the condensate compared to the density modes
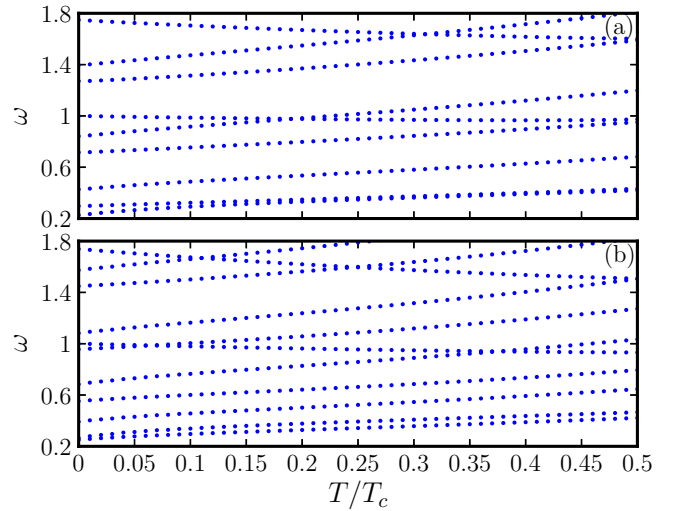

FIG. 12. Excitation spectrum of the ^{23}Na spin-1 BEC at finite temperature with $c_0 = 0.001\,19N$, $c_2 = 0.000\,424N$, $\gamma = 0.5$, and (a) $N = 2000$ and (b) $N = 4000$.

such as breathing and dipole modes. The former decrease with an increase in the number of atoms, whereas the latter remain almost unchanged. The spin modes therefore increase with an increase of temperature as the number of atoms in the condensate is decreasing. The density modes, on other hand, are more sensitive to change in the effective potential due to the thermal cloud. In order to further ascertain the role of the thermal cloud for the density modes, we extend the variational analysis of Sec. III E to finite temperatures [67] for a density-breathing mode. We assume the thermal cloud as a static classical gas and write [67]

$$\tilde{n}_i = r(T) \exp[-V(x)/k_B T], \quad (26)$$

where $r(T)$ is the normalization constant. The thermal-cloud density is normalized as $\int \sum_i dx\, \tilde{n}_i(x) = N_T$, where N_T is the number of atoms in the thermal cloud. The energy with the thermal cloud's contribution included can be written as $E + E_T$, where

$$E_T = [(c_0 + c_2)(\tilde{n}_{+1}|\phi_{+1}|^2 + \tilde{n}_{-1,-1}|\phi_{-1}|^2)$$
$$+ (c_0 - c_2)(\tilde{n}_{+1}|\phi_{-1}|^2 + \tilde{n}_{-1,-1}|\phi_{+1}|^2)] \quad (27)$$

and E is defined in Eq. (19). Replacing E by $E + E_T$ in the Lagrangian (18) and using the ansatz (17), the linearized equation of motion for the condensate width σ is

$$\ddot{\delta\sigma}(t) + \left(1 + \frac{3}{\sigma^4} + \sqrt{\frac{2}{\pi}} \frac{c_0}{\sigma^3} - f(T)\right)\delta\sigma(t) = 0, \quad (28)$$

where $f(T) = \sqrt{\frac{1}{2\pi}} c_0 N_T / (k_B T)^{3/2}$ and the condensate width has been considered to be much smaller than the width of the thermal cloud. The frequency of the density-breathing mode from Eq. (28) is

$$\omega_b = \left[1 + \frac{3}{\sigma^4} + \sqrt{\frac{2}{\pi}} \frac{c_0}{\sigma^3} - f(T)\right]^{1/2}, \quad (29)$$

where $f(T)$ results in the decrease in ω_b as a function of temperature T.

V. CONCLUSION

In this work we have investigated the collective excitations of a quasi-one-dimensional interacting SO-coupled spin-1 BEC with antiferromagnetic spin-exchange interactions at zero and finite temperatures by employing the HFB-Popov approximation. In this approximation, the static properties of the system are very well described by GP equations which are coupled to BdG equations. Although, as per the Popov approximation, we have neglected the anomalous average terms in the generalized GP equations and the BdG equations, we have included and illustrated the importance of the coherence terms between the thermal atoms of different components. The low-lying modes of the interacting spin-1 BEC in the absence of SO coupling are characterized by the three Goldstone modes and doubly degenerate spin modes. With the introduction of an SO coupling, the degeneracy between the two spin modes is lifted, where one of the modes increases with an increase in SO coupling strength while the other remains unchanged. We calculated the dispersion curves, showing explicitly that the energy of density excitations is always higher than that of the corresponding spin excitations and, moreover, in the presence of SO coupling, dispersion has three distinct branches consistent with a breakdown in the degeneracy of the spin modes. To substantiate our theoretical prediction of the low-lying modes through physical observables useful for experiments, we performed dynamical real-time simulations of the system by evolving the ground state in the presence of perturbations. We indeed found that the dominant frequencies of oscillation in the center of mass and mean-square radius in both the spin and density channels are in excellent agreement with the Bogoliubov calculations. Considering a pseudospinor subsystem, we also carried out a time-dependent variational analysis and demonstrated that the analytical and numerical results match quite well with each other. The collective excitations and equilibrium density profiles at nonzero temperatures were also presented. While the energy of the density modes decreases with an increase in temperature, the energy of the spin modes increases. A natural extension of this work would be to compute systematically the phase diagram of the interacting SO-coupled spin-1 BEC and to study the dynamics of the collective excitation at finite temperatures.

[1] D. M. Stamper-Kurn, M. R. Andrews, A. P. Chikkatur, S. Inouye, H.-J. Miesner, J. Stenger, and W. Ketterle, Phys. Rev. Lett. **80**, 2027 (1998).

[2] M. D. Barrett, J. A. Sauer, and M. S. Chapman, Phys. Rev. Lett. **87**, 010404 (2001).

[3] M.-S. Chang, C. D. Hamley, M. D. Barrett, J. A. Sauer, K. M. Fortier, W. Zhang, L. You, and M. S. Chapman, Phys. Rev. Lett. **92**, 140403 (2004).

[4] T. Kuwamoto, K. Araki, T. Eno, and T. Hirano, Phys. Rev. A **69**, 063604 (2004).

[5] H. Schmaljohann, M. Erhard, J. Kronjäger, M. Kottke, S. van Staa, L. Cacciapuoti, J. J. Arlt, K. Bongs, and K. Sengstock, Phys. Rev. Lett. **92**, 040402 (2004).

[6] Y. Kawaguchi and M. Ueda, Phys. Rep. **520**, 253 (2012).

[7] D. M. Stamper-Kurn and M. Ueda, Rev. Mod. Phys. **85**, 1191 (2013).

[8] Y.-J. Lin, K. Jiménez-García, and I. B. Spielman, Nature (London) **471**, 83 (2011).

[9] M. Z. Hasan and C. L. Kane, Rev. Mod. Phys. **82**, 3045 (2010).

[10] E. van der Bijl and R. A. Duine, Phys. Rev. Lett. **107**, 195302 (2011).

[11] H. Zhai, Rep. Prog. Phys. **78**, 026001 (2015).

[12] D. Campbell, R. Price, A. Putra, A. Valdés-Curiel, D. Trypogeorgos, and I. Spielman, Nat. Commun. **7**, 10897 (2016).

[13] X. Luo, L. Wu, J. Chen, Q. Guan, K. Gao, Z.-F. Xu, L. You, and R. Wang, Sci. Rep. **6**, 18983 (2016).

[14] C. Wang, C. Gao, C.-M. Jian, and H. Zhai, Phys. Rev. Lett. **105**, 160403 (2010).

[15] G. I. Martone, F. V. Pepe, P. Facchi, S. Pascazio, and S. Stringari, Phys. Rev. Lett. **117**, 125301 (2016).

[16] L. Chen, H. Pu, Z.-Q. Yu, and Y. Zhang, Phys. Rev. A **95**, 033616 (2017).

[17] B. A. Malomed, Europhys. Lett. **122**, 36001 (2018).

[18] K. Kasamatsu, M. Tsubota, and M. Ueda, Int. J. Mod. Phys. B **19**, 1835 (2005).

[19] C. J. Pethick and H. Smith, *Bose-Einstein Condensation in Dilute Gases* (Cambridge University Press, Cambridge, 2008).

[20] L. Pitaevskii and S. Stringari, *Bose-Einstein Condensation and Superfluidity* (Oxford University Press, Oxford, 2016), Vol. 164.

[21] M.-O. Mewes, M. R. Andrews, N. J. van Druten, D. M. Kurn, D. S. Durfee, C. G. Townsend, and W. Ketterle, Phys. Rev. Lett. **77**, 988 (1996).

[22] Y. Li, G. I. Martone, L. P. Pitaevskii, and S. Stringari, Phys. Rev. Lett. **110**, 235302 (2013).

[23] Z.-Q. Yu, Phys. Rev. A **93**, 033648 (2016).

[24] K. Sun, C. Qu, Y. Xu, Y. Zhang, and C. Zhang, Phys. Rev. A **93**, 023615 (2016).

[25] T. Ozawa, L. P. Pitaevskii, and S. Stringari, Phys. Rev. A **87**, 063610 (2013).

[26] M. A. Khamehchi, Y. Zhang, C. Hamner, T. Busch, and P. Engels, Phys. Rev. A **90**, 063624 (2014).

[27] S.-C. Ji, L. Zhang, X.-T. Xu, Z. Wu, Y. Deng, S. Chen, and J.-W. Pan, Phys. Rev. Lett. **114**, 105301 (2015).

[28] M. Tylutki, G. E. Astrakharchik, B. A. Malomed, and D. S. Petrov, Phys. Rev. A **101**, 051601(R) (2020).

[29] T. Isoshima, T. Ohmi, and K. Machida, J. Phy. Soc. Jpn. **69**, 3864 (2000).

[30] W. Zhang, S. Yi, and L. You, Phys. Rev. A **70**, 043611 (2004).

[31] N. T. Phuc, Y. Kawaguchi, and M. Ueda, Phys. Rev. A **84**, 043645 (2011).

[32] Y. Kawaguchi, N. T. Phuc, and P. B. Blakie, Phys. Rev. A **85**, 053611 (2012).

[33] D. Jacob, L. Shao, V. Corre, T. Zibold, L. De Sarlo, E. Mimoun, J. Dalibard, and F. Gerbier, Phys. Rev. A **86**, 061601(R) (2012).

[34] J. Mur-Petit, M. Guilleumas, A. Polls, A. Sanpera, M. Lewenstein, K. Bongs, and K. Sengstock, Phys. Rev. A **73**, 013629 (2006).

[35] M. Moreno-Cardoner, J. Mur-Petit, M. Guilleumas, A. Polls, A. Sanpera, and M. Lewenstein, Phys. Rev. Lett. **99**, 020404 (2007).

[36] E. Witkowska, T. Świsłocki, and M. Matuszewski, Phys. Rev. A **90**, 033604 (2014).

[37] X.-L. Chen, X.-J. Liu, and H. Hu, Phys. Rev. A **96**, 013625 (2017).

[38] S.-C. Ji, J.-Y. Zhang, L. Zhang, Z.-D. Du, W. Zheng, Y.-J. Deng, H. Zhai, S. Chen, and J.-W. Pan, Nat. Phys. **10**, 314 (2014).

[39] Z.-Q. Yu, Phys. Rev. A **90**, 053608 (2014).

[40] T. Ozawa and G. Baym, Phys. Rev. Lett. **109**, 025301 (2012).

[41] E. Kawasaki and M. Holzmann, Phys. Rev. A **95**, 051601(R) (2017).

[42] S.-W. Su, I.-K. Liu, S.-C. Gou, R. Liao, O. Fialko, and J. Brand, Phys. Rev. A **95**, 053629 (2017).

[43] R. M. Wilson, S. Ronen, and J. L. Bohn, Phys. Rev. Lett. **104**, 094501 (2010).

[44] T.-L. Ho, Phys. Rev. Lett. **81**, 742 (1998).

[45] T. Ohmi and K. Machida, J. Phy. Soc. Jpn. **67**, 1822 (1998).

[46] A. Griffin, Phys. Rev. B **53**, 9341 (1996).

[47] A. Roy, S. Gautam, and D. Angom, Phys. Rev. A **89**, 013617 (2014).

[48] A. Roy and D. Angom, Phys. Rev. A **90**, 023612 (2014).

[49] N. M. Hugenholtz and D. Pines, Phys. Rev. **116**, 489 (1959).

[50] P. Kaur, A. Roy, and S. Gautam, Comput. Phys. Commun. **259**, 107671 (2021).

[51] P. Banger, P. Kaur, and S. Gautam, Int. J. Mod. Phys. C **33**, 2250046 (2022).

[52] Y. Gao and Y. Cai, J. Comput. Phys. **403**, 109058 (2020).

[53] E. Serrano-Ensástiga and F. Mireles, Phys. Rev. A **104**, 063308 (2021).

[54] C. Ticknor, Phys. Rev. A **89**, 053601 (2014).

[55] S. Pal, A. Roy, and D. Angom, J. Phys. B **51**, 085302 (2018).

[56] S. Knoop, T. Schuster, R. Scelle, A. Trautmann, J. Appmeier, M. K. Oberthaler, E. Tiesinga, and E. Tiemann, Phys. Rev. A **83**, 042704 (2011).

[57] H. Watanabe and H. Murayama, Phys. Rev. Lett. **108**, 251602 (2012).

[58] J. F. Dobson, Phys. Rev. Lett. **73**, 2244 (1994).

[59] T. Bienaimé, E. Fava, G. Colzi, C. Mordini, S. Serafini, C. Qu, S. Stringari, G. Lamporesi, and G. Ferrari, Phys. Rev. A **94**, 063652 (2016).

[60] V. M. Pérez-García, H. Michinel, J. I. Cirac, M. Lewenstein, and P. Zoller, Phys. Rev. Lett. **77**, 5320 (1996).

[61] V. M. Pérez-García, H. Michinel, J. I. Cirac, M. Lewenstein, and P. Zoller, Phys. Rev. A **56**, 1424 (1997).

[62] W. Ketterle and N. J. van Druten, Phys. Rev. A **54**, 656 (1996).

[63] Y.-M. Kao and T. F. Jiang, Eur. Phys. J. D **40**, 263 (2006).

[64] W.-J. Huang, S.-C. Gou, and Y.-C. Tsai, Phys. Rev. A **65**, 063610 (2002).

[65] C. Gies, B. P. van Zyl, S. A. Morgan, and D. A. W. Hutchinson, Phys. Rev. A **69**, 023616 (2004).

[66] R. J. Dodd, M. Edwards, C. W. Clark, and K. Burnett, Phys. Rev. A **57**, R32(R) (1998).

[67] H. Shi and W.-M. Zheng, Phys. Rev. A **59**, 1562 (1999).